

Investigation of the parallel gradation method based on the response of track-bed materials under cyclic loadings

Shuai Qi, Yu Jun Cui, Jean Claude Dupla, Ren-Peng Chen, Han-Lin Wang,
Yu Su, Francisco Lamas-Lopez, Jean Canou

► To cite this version:

Shuai Qi, Yu Jun Cui, Jean Claude Dupla, Ren-Peng Chen, Han-Lin Wang, et al.. Investigation of the parallel gradation method based on the response of track-bed materials under cyclic loadings. *Transportation Geotechnics*, Elsevier, 2020, 24, pp.100360. 10.1016/j.trgeo.2020.100360 . hal-03045872

HAL Id: hal-03045872

<https://hal-enpc.archives-ouvertes.fr/hal-03045872>

Submitted on 28 May 2021

HAL is a multi-disciplinary open access archive for the deposit and dissemination of scientific research documents, whether they are published or not. The documents may come from teaching and research institutions in France or abroad, or from public or private research centers.

L'archive ouverte pluridisciplinaire **HAL**, est destinée au dépôt et à la diffusion de documents scientifiques de niveau recherche, publiés ou non, émanant des établissements d'enseignement et de recherche français ou étrangers, des laboratoires publics ou privés.

1 **Investigation of the parallel gradation method based on the response of**
2 **track-bed materials under cyclic loadings**

3

4 Shuai Qi^{1,2}, Yu-Jun Cui², Jean-Claude Dupla², Ren-Peng Chen¹, Han-Lin Wang³, Yu
5 Su², Francisco Lamas-Lopez², Jean Canou²

6

7 1: Zhejiang University, China

8 2: Laboratoire Navier/CERMES, Ecole des Ponts ParisTech (ENPC), France

9 3: Department of Civil and Environmental Engineering, The Hong Kong Polytechnic
10 University, Hung Hom, Kowloon, Hong Kong, China

11

12

13

14

15

16

17

18 **Corresponding author:**

19 Mr. Shuai Qi

20 Department of Civil Engineering

21 Zhejiang University, Hangzhou, China

22 E-mail: qishuailw@163.com

23 **Abstract**

24 Ballast/fines mixture is often found in railway substructure and the overall behaviour
25 of tracks is strongly dependent on the mechanical behaviour of this mixture. Since
26 directly testing such mixture with large grains is limited with common laboratory
27 equipment, the consideration of a model material at smaller size is advisable. Parallel
28 gradation method is widely used for this purpose. This study assesses the validity of
29 this method in the case of ballast/fines mixture. Large-scale cyclic triaxial tests were
30 carried out on the ballast/fines mixture at six volumetric coarse grain contents. The
31 results obtained were analysed, together with those obtained previously from
32 small-scale triaxial tests on a microballast/fines mixture whose microballast grain size
33 distribution was determined by applying the parallel gradation method. The cyclic
34 parameters (permanent strain and resilient modulus) were obtained for the two types
35 of mixture. Results show that for all mixtures two distinct soil fabrics can be
36 identified according to the variations of permanent strain and resilient modulus with
37 the volumetric content of coarse grains f_v : a fine-fine contact structure for $f_v \leq 20\%$
38 and a grain-grain contact structure for $f_v \geq 35\%$. In the case of fine-fine contact
39 structure, the permanent strains and resilient modulus values of the ballast specimens
40 are consistent with those of the microballast specimens, evidencing the validity of the
41 parallel gradation method. In the case of grain-grain contact structure, the permanent
42 strains and resilient modulus values are found to coincide globally at the two scales,
43 also justifying the validity of the parallel gradation method, the slight differences
44 between the two scales being attributed to the irregular grain sliding and the

45 distribution of the fines soils.

46

47 **Keywords:** interlayer soil; cyclic triaxial tests; permanent deformation; resilient

48 modulus; parallel gradation method

49 **1. Introduction**

50 Ballast/fines mixture is often found in railway substructure [10,17]. For instance, in
51 the French conventional railway lines (representing 94% of the total railway network),
52 there is an interlayer which was formed by interpenetration of ballast and subgrade
53 soils under the effect of train circulation [10]. During the renewable program for
54 conventional lines, this layer was maintained since the dry density of the interlayer
55 was as high as 2.4 Mg/m^3 and thus a favourable mechanical behaviour was expected
56 [7]. According to the in-situ investigation, the soil fabric of the interlayer is found to
57 be greatly dependent on the content of ballast grains [37,38]: the ballast grains are in
58 contact with each other for the upper part with high ballast content, but floated in the
59 fines matrix for the lower part with lower ballast content. Since the ballast/fines
60 mixture plays an important role in the overall behaviour of rail tracks, it is important
61 to investigate the mechanical response of such mixture under cyclic loading in terms
62 of permanent deformation and resilient modulus. Considering the large size of ballast
63 grains, large-scale triaxial apparatus is normally needed for this purpose. However,
64 since the large testing system is complex and costly, scaling the ballast grains down to
65 a model ballast material with smaller size and performing tests using standard
66 apparatus appear quite promoting.

67 Three methods are commonly used for the scaling purpose: the scalping method
68 [50] which consists in discarding the grains larger than a specified size from the
69 prototype materials, the parallel gradation method [24] which consists in creating a
70 model material at smaller size with its grain size distribution parallel to that of the

71 prototype material, and the replacement method [14] which consists in replacing the
72 grains from a specified size to the maximum size with the grains from this specified
73 size to a smaller size. Among them, the parallel gradation method is regarded to be the
74 most appropriate because it can consider a large range of prototype gradation shape;
75 thus, it has been adopted mostly [1,16,29,39,42,43,44,47]. The validity of this method
76 under cyclic loadings was assessed by Sevi and Ge [34] based on the response of the
77 prototype and model grains of ballast grains. Their results in terms of resilient
78 modulus, permanent axial strain and permanent volumetric strain were unfortunately
79 not conclusive for validating the parallel gradation method. In addition, only pure
80 ballast grains were tested without fines fraction.

81 In this study, the parameters characterizing the cyclic response (permanent
82 strain and resilient modulus) of ballast/fines mixtures representing the interlayer soils
83 in the conventional French railway track-beds were determined by conducting
84 large-scale cyclic triaxial tests. Six volumetric ballast contents (0%, 5%, 10%, 20%,
85 35%, 45%) were considered. The results obtained were analysed together with those
86 obtained previously by Wang et al. [42,43] from small-scale cyclic triaxial tests on
87 microballast/fines mixture with microballast prepared by applying the parallel
88 gradation method. Comparison of the mechanical parameters obtained at two scales
89 allowed the validity of the parallel gradation method to be assessed on coarse
90 grain/fines mixtures.

91

92 **2. Materials**

93 The ballast grains having the same grain size distribution as the interlayer soil in
94 “Sénissiat site” were used [37], as shown in Fig. 1. The minimum grain size D_{\min}^b
95 and the maximum grain size D_{\max}^b are 20 mm and 63 mm, respectively. The
96 microballast was tested previously by Wang et al. [42,43]; its maximum grain size
97 D_{\max}^m was chosen as 20 mm to adapt to a small-scale triaxial cell of 100 mm with a
98 value of 5 as the ratio of specimen to maximum grain size. This is consistent with the
99 recommendation of Fagnoul and Bonnechere [12], Nitchiporovitch [25] and Pedro
100 [28]: a ratio larger than 5 must be adopted to minimize the specimen size effect. The
101 grain size distribution of the microballast is transited from that of the ballast by
102 following the parallel gradation method. In this method, the correlative grain sizes of
103 ballast and microballast share the same percentage of grain passing. The grain sizes of
104 these two materials are correlated according to the following equation:

105 (1)
$$\frac{D^b - D_{\min}^b}{D^m - D_{\min}^m} = \frac{D_{\max}^b - D_{\min}^b}{D_{\max}^m - D_{\min}^m} = A$$

106 where D_{\max} , D_{\min} and D are the maximum grain size, the minimum grain size, and a
107 given grain size, respectively. The superscripts b and m stand for ballast and
108 microballast, respectively. A is a constant.

109 To prepare the microballast, three angular-shaped commercial coarse grains
110 were used. Visually, the grain shape of the chosen commercial grains was similar to
111 that of the field ballast from “Sénissiat site”. The minimum grain size of the
112 commercial grains D_{\min}^m was 1.6 mm, defining a value of 2.337 for parameter A . For
113 a given grain size of microballast D^m , 10.0 mm for instance, equation (1) gives a

114 correlated ballast grain size D^b of 39.6 mm. As the ballast grain passing percentage
115 is 59.1 % for $D^b = 39.6$ mm, according to the parallel gradation method, the
116 microballast grain passing percentage is also 59.1 % for $D^m = 10$ mm. Following this
117 procedure, the complete grain size distribution of the microballast was obtained, as
118 shown in Fig. 1. This target (parallel gradation) curve was verified by measurement
119 and it is observed that the measured grain size distribution and the target one show a
120 good agreement (Fig. 1).

121 For the fines soils, since obtaining enough quantity from the field was difficult,
122 they were fabricated in the laboratory. Nine commercial soils were mixed to simulate
123 the fines soils from “Sénissiat site”, which included five kinds of medium sands, two
124 kinds of fine sands and two kinds of clay soils (kaolinite and bentonite). Table 1 listed
125 the properties of these soils. The mass proportion of each constituting soil was
126 calculated according to the grain-size distributions of the fines from “Sénissiat site”
127 (Fig. 2). The calculated results were also shown in Table 1. With the proportion and
128 the grain size distribution of each soil, the grain size distribution of the fabricated
129 fines can be calculated, which was plotted in Fig. 2 as well. During the mixing
130 procedure, the materials to be mixed were carefully added into the mixer following
131 the sequence of medium sands, water, fine sands, kaolinite and bentonite. The mass of
132 the added water corresponded to a small water content of 4% of the total mixed soils.
133 The aim of water addition was to prevent the small particles loss during the mixing,
134 occurring when fine sands, kaolinite and bentonite were dry mixed with others.
135 Bentonite was added last since it was the most reactive soil with water. With this

136 sequence, most kaolinite and bentonite particles were expected to be adhered to the
137 surface of sands. Using this procedure, a homogeneous mixture can be obtained [21].
138 Wang et al. [42,43] also adopted this method when preparing specimens of
139 microballast and fines mixture. After preparation, the fabricated fines soil was
140 compared with the field one in terms of grain size distribution and plasticity. As can
141 be observed from Fig. 2, the grain size distribution of the fabricated fines showed a
142 good agreement with that of the in situ one. In addition, the liquid limit and the
143 plasticity index of the fabricated fines, which were 32% and 20%, respectively,
144 matched the target liquid limit (35.5%) and plasticity index (17.3%) well. This soil is
145 classified as lean clay (CL) according to ASTM D2487-11 [3]. Standard Proctor
146 compaction tests were carried out on the fines material following ASTM D698-12 [4].
147 An optimum water content $w_{opt-f} = 13.70\%$ and a maximum dry density $\rho_{dmax-f} = 1.82$
148 Mg/m^3 were determined.

149

150 **3. Experimental methods**

151 **3.1. Specimen preparation**

152 In order to quantify the coarse grains in a specimen, a parameter namely volumetric
153 content of coarse grains f_v was adopted, which was defined as the ratio of the total
154 volume of coarse grains to the total specimen volume [28,29,32,42,43,44]. The total
155 specimen volume consisted of two parts: the coarse grain volume and the fines
156 volume. All pores were assumed to be included in the fines soils. For the upper part of
157 the natural interlayer soils at “Sénissiat site”, the f_v value was 52.9% [37]. In this

158 study, six f_v values (0%, 5%, 10%, 20%, 35%, 45%) were considered for the
159 specimens prepared with both ballast and microballast. For convenience, in further
160 analysis, the specimens prepared with ballast and microballast are referred to as
161 ballast specimens and microballast specimens, respectively. The dimensions of the
162 ballast specimens are 300 mm diameter and 600 mm height, while the dimensions of
163 microballast specimens are 100 mm diameter and 200 mm height.

164 For the preparation of the ballast specimen, the total volume was first calculated
165 with the specimen dimensions (300 mm diameter and 600 mm height). For a given f_v
166 value, the volumes of both ballast grains and fines can be obtained based on this total
167 specimen volume. After that, the mass of ballast was obtained using the dry unit mass
168 of ballast (2.68 Mg/m³). The fines in all specimens were kept at the same state defined
169 by the optimum water content $w_{\text{opt-f}} = 13.70\%$ and the maximum dry density $\rho_{\text{dmax-f}} =$
170 1.82 Mg/m³. The optimum state was selected aiming to simulate the heavily compact
171 state in the field condition [8,21,38]. Accordingly, the masses of dry fines and water
172 can be determined. Water was firstly added into the fines by spray to reach the
173 optimum water content $w_{\text{opt-f}} = 13.7\%$. Then, the wetted fines soil was stored in
174 hermetic containers for 24 h for moisture homogenization. Afterwards, the
175 homogenized wetted fines soil was equally divided into eight parts (by weight) and so
176 were the oven-dried ballast grains, after which they were mixed separately. Finally,
177 the ballast specimen was compacted using a layered compaction method, which was
178 widely adopted by many researchers to ensure reasonable uniformity of the specimen
179 [5,22,35,46]. The mixed materials were compacted in eight layers using a vibration

180 hammer, each with a thickness of 75 mm.

181 Similar protocol was applied for the preparation of the microballast specimen
182 (100 mm diameter and 200 mm height). The masses of the dry microballast, dry fines
183 soil and water were firstly determined. Afterwards, the fines soil was wetted with the
184 sprayed water to reach the optimum water content of 13.7%, stored in hermetic
185 container for 24 h and then mixed with the microballast. Finally, this mixture was
186 compacted dynamically to reach the target height, also following the layered
187 compaction method to ensure reasonable uniformity of the specimen. More details can
188 be found in Wang et al. [42,43]. Note that the test results at five f_v values (5%, 10%,
189 20%, 35%, 45%) obtained by Wang et al. [42,43] were taken for comparison with the
190 corresponding ones of the ballast samples in this study.

191

192 **3.2. Cyclic triaxial tests**

193 For the microballast specimen with 100 mm diameter and 200 mm height, a
194 small-scale cyclic triaxial apparatus was used. Details about this device can be found
195 in Wang et al. [43]. For testing a ballast specimen (300 mm diameter and 600 mm
196 height), a large-scale cyclic triaxial apparatus developed by Dupla et al. [11] was
197 adopted. The loading procedures adopted are the same for the ballast and the
198 microballast specimens. No saturation process was applied and the specimen water
199 content was kept constant during the test. In addition, the drainage valve was kept
200 open during the loading process. All the tests were performed at a confining pressure
201 of 30 kPa, which corresponded to the average horizontal stress estimated for the field

202 condition, considering the effects of the train wheel load, the interlayer depth and the
203 Poisson ratio [9,42,43]. The applied cyclic loads followed a sine-shaped pattern (Fig.
204 3). The deviator stress amplitude Δq is defined as the difference value between the
205 maximum deviator stress q_{max} and the minimum deviator stress q_{min} [40,41,42,43]. A
206 frequency of 1.78 Hz corresponding to a low train speed of 50 km/h was chosen,
207 aiming to guarantee the quality of controlling the pre-defined loading shape. Note that
208 this low frequency did not reflect the high train speed normally encountered in the
209 field. This selection was based on the hypothesis that the train speed does not
210 influence the assessment of the validity of the parallel gradation. During the loading
211 procedure, axial stress and strain were monitored.

212 The application of cyclic loads included two consecutive stages. The loading
213 stage 1 was focused on the aspect of the permanent deformation under a large number
214 of loading cycles. The loading stage 2 was focused on the aspect of the resilient
215 modulus or stiffness property under a wide range of stress amplitudes, including some
216 large amplitudes possibly applied on the interlayer soils. In stage 1, a multi-step
217 loading procedure proposed by Gidel et al. [13] was adopted (Fig. 4a): the deviator
218 stress amplitude $\Delta q = q_{max} - q_{min}$ was increased stepwise from 10 kPa to 30 kPa with
219 an increment of 5 kPa. At each amplitude, 90,000 cycles were applied, which were
220 thought to be enough for the stabilization of the permanent strain [10,13,21,38]. This
221 multi-stage loading procedure allowed the application of several stress amplitudes on
222 the same specimen, with which not only the number of tests could be reduced, but
223 also the effect of the variability of soil specimens on the testing results can be

224 minimised. Thus, this procedure has been widely used in the study of the permanent
225 deformation behaviour [6,10,19,21,36,38,43]. These loading amplitudes were selected
226 based on the vertical stress measured at the equivalent depth of interlayer in the field
227 [20,21]. In stage 2 (Fig. 4b), a procedure proposed by Lamas-Lopez [23] was adopted.
228 The deviator stress amplitude Δq was firstly increased following a Δq sequence (10
229 kPa, 30 kPa and 50 kPa) and then decreased following the reverse sequence.
230 Afterwards, Δq was increased following a sequence from 10 kPa to 100 kPa and then
231 decreased to 10 kPa. Finally, Δq was increased in steps to 200 kPa and then decreased
232 to 10 kPa. At each stress level, 100 cycles were applied. The aim of firstly increasing
233 Δq and then decreasing it was to obtain the resilient modulus at both elastoplastic
234 stage and pure elastic stage. Note that the large stress amplitudes (50 kPa, 100 kPa
235 and 200 kPa) were defined according to the vertical stress of 40-90 kPa at similar
236 depth of the interlayer observed by Selig and Waters [33], Jain and Keshav [18] and
237 Yang et al. [49], the vertical stress of 120-138 kPa applied by heavier wagons in some
238 countries [15,18,23] and the contingent maximum vertical stress at the top of railway
239 structure as high as 200 kPa [21].

240

241 **4. Results and discussions**

242 **4.1. Variations of permanent deformation with f_v**

243 Fig. 5 plots the deviator stress q versus the axial strain ε_1 during the first 90,000
244 cycles of loading stage 1 for the ballast specimen at $f_v = 35\%$. In a loading-unloading
245 cycle, the permanent axial strain ε_{1p} represented the irreversible part of the total

246 axial strain. It can be observed that the ε_{1p} value of the first cycle was particularly
247 large. This phenomenon was also observed for other ballast specimens and the
248 microballast specimens. This large permanent strain can be attributed to the
249 adaptation of the specimen to the loading system, in particular in terms of contact
250 between the specimen and the loading piston. As the initial specimen-piston contact
251 was not identical for all the specimens, this ε_{1p} value would make impossible the
252 relevant comparison of permanent strain ε_{1p} between different specimens. Thus, in further
253 analysis, the first cycle was not accounted for the cumulative permanent strain.

254 Fig. 6 presents the permanent strain ε_{1p} against the number of cycles N for six
255 ballast specimens, with the corresponding stress levels. The evolutions of permanent
256 strain with number of cycles N were the same as the ones of microballast specimens
257 [43]. It can be observed from Fig. 6 that for each f_v value, ε_{1p} increased quickly at the
258 start of each loading level and then tended to stabilize with the increasing cycles.
259 According to Werkmeister et al. [45], the large deformation in the beginning resulted
260 from a significant rearrangement of the particles. As the cycle number increased, this
261 particle rearrangement became more and more limited, and correspondingly, the
262 permanent strain tended to become stable. As can also be seen from Fig. 6, a
263 smaller f_v value led to a larger ε_{1p} , which can be attributed to the involvement of less
264 coarse grains.

265 Due to the multi-step loading procedure adopted, the ε_{1p} at each stress level
266 was greatly influenced by the previous loadings (Fig. 6). If this loading history is
267 eliminated (as if the specimen has been subjected to only one loading level), the effect

268 of the ballast contents can be better evaluated. For this purpose, a permanent strain
269 estimation method proposed by Gidel et al. [13] and then used by Lamas-Lopez [21]
270 and Wang et al. [43] was adopted. The application of this method is explained in Fig.
271 7 by considering two successive loading levels (Loading level M and Loading level M
272 + 1). For the estimated permanent strain ε_{1p}^{M+1} of the Loading level $M + 1$ at the first
273 90,000 cycles, it is determined as:

$$274 \quad (2) \quad \varepsilon_{1p}^{M+1} = \varepsilon_{1p}^M + \delta\varepsilon_{1p}^{M+1}$$

275 where ε_{1p}^M is the measured permanent strain of the Loading Level M ; $\delta\varepsilon_{1p}^{M+1}$ is the
276 translated permanent strain determined by resetting both the initial strain value and
277 the first cycle of the measured permanent strain of the Loading level $M + 1$ to 0.

278 For estimating the permanent strain of the Loading level $M + 1$ after 90,000
279 cycles, a linear increasing trend between permanent strain and number of cycles is
280 considered, with its slope kept at the same value as the one determined at the last
281 cycles of Loading level $M + 1$. More details can be found in Wang et al. [43].

282 The estimated permanent strain curves for $f_v = 0\%$ of the ballast specimen are
283 presented in Fig. 8, together with the measured results. It can be observed that at the
284 last cycle of each stress level, the estimated strain was larger than the measured one.
285 For example, for $\Delta q = 20$ kPa, the measured permanent strain at the last cycle $N =$
286 270,000 was 0.182%, while the corresponding estimated one was 0.226%. This
287 phenomenon can be attributed to the different loading histories: for the estimated
288 strain, the specimen was assumed to undergo one higher stress level of 20 kPa. When
289 it came to the measured strain, successive lower stress levels of 10kPa, 15 kPa and 20

290 kPa were applied, leading to a smaller strain value.

291 Gidel et al. [13] examined this permanent strain estimation method through
292 cyclic triaxial tests, concluding that the permanent strain estimated for a single stress
293 level agreed well with the measured one for the loading cycles applied at each step
294 (90,000 cycles in this study). In other words, in this study, the estimated permanent
295 strain at the first 90,000 cycles was relatively accurate. Fig. 9 depicts the estimated
296 permanent strain evolutions at the first 90,000 cycles under different stress levels for
297 ballast specimen at $f_v = 0\%$. As can be observed, a larger stress level led to a larger
298 strain value. In addition, the permanent strain gradually stabilized with the increase of
299 the cycle number. To further illustrate the effect of ballast content f_v , the estimated
300 permanent strains for cycle $N = 90,000$ (end-stage cycle in Fig. 9) at all stress levels
301 were taken and compared (Fig. 10). It can be observed that at each stress level, the
302 permanent strain decreased with the increase of f_v . Moreover, a bi-linear decreasing
303 trend could be identified. When $f_v \leq 20\%$, the permanent strain decreased rapidly. By
304 contrast, when $f_v \geq 35\%$, this decreasing rate became smaller. The same observations
305 were made by Wang et al. [43] for the microballast specimens.

306 In the study of Wang et al. [43], X-ray microcomputed tomography (μ CT) scans
307 were carried out on the as-compacted microballast specimens. Two soil fabrics were
308 identified at different f_v values: a fine-fine contact structure at $f_v = 0\%$ - 20% and a
309 distinct grain-grain contact structure at $f_v = 35\%$ - 45% . It is worth noting that at $f_v =$
310 20% , the coarse grains started to be partially connected without forming a whole
311 skeleton. Unfortunately, this μ CT scan could not be conducted on ballast specimens

312 due to their large size. However, basically, it seems plausible to consider the same
313 feature of fabrics for the ballast specimens: also a fine-fine contact structure at low f_v
314 and a grain-grain contact structure at high f_v . For fine-fine contact structure, the
315 permanent strain results from the compression of the fines, which decreases rapidly
316 with increasing f_v . By contrast, for grain-grain contact structure, the rearrangement of
317 the grains plays a dominant role and the permanent strain decreases slightly when f_v
318 increases.

319

320 **4.2. Variations of resilient modulus with f_v**

321 Typical hysteresis loops at the first cycles of different stress levels are shown in Fig.
322 11 for the ballast specimen at $f_v = 20\%$. The loops for stress levels of $\Delta q = 10$ kPa, Δq
323 $= 30$ kPa, $\Delta q = 50$ kPa, $\Delta q = 100$ kPa and $\Delta q = 200$ kPa corresponded to cycle
324 numbers of $N = 1$, $N = 101$, $N = 201$, $N = 701$ and $N = 1401$, respectively. It appears
325 that for the low stress levels of 10 kPa and 30 kPa, the hysteresis loops were pretty
326 small and closed. This was due to the application of 450,000 loading cycles under Δq
327 ≤ 30 kPa in loading stage 1. By contrast, for stress levels larger than 30 kPa,
328 permanent strain developed, leading to larger and unclosed hysteresis loops, in
329 particular under stress levels as high as $\Delta q = 100$ kPa and 200 kPa.

330 The evolution of hysteresis loop with number of cycles is illustrated in Fig. 12
331 by plotting the loops for 100 cycles (from $N = 701$ to $N = 800$) at $\Delta q = 100$ kPa for
332 the ballast specimen with $f_v = 20\%$. A large and unclosed hysteresis loop was observed
333 for the first cycle, due to the stress level of 100 kPa which was larger than all the

334 previous applied stress levels. In addition, with the increase of the cycle number, the
335 hysteresis loop became smaller and smaller and at the end of loading, the loops
336 became closed and relatively unchanged, suggesting a pure elastic behaviour of soil.

337 As shown in Fig. 13, the resilient modulus M_r is defined as [30,31]:

338 (3)
$$M_r = \Delta q / \varepsilon_{1r}$$

339 where Δq is the deviator stress amplitude, and ε_{1r} is the resilient strain.

340 The evolution of M_r with the number of cycles N at varying stress levels is
341 presented in Fig. 14 for the ballast specimen at $f_v = 20\%$. The results of other ballast
342 specimens and microballast specimens obey the same rule and are not shown for
343 clarity. It can be observed that when the stress amplitude increased, the M_r value
344 immediately decreased and then tended to stabilize. By contrast, with the stress
345 amplitude decreasing, the M_r value increased instantly and then tended to reach a
346 stabilization state. The decrease of M_r with the increase of stress amplitude can be
347 explained by the strain increasing due to the increase of stress amplitude [2].

348 In order to illustrate the effect of f_v on resilient modulus, the M_r values of the
349 last (end-stage) cycles of all stress levels were taken and presented as a function of f_v
350 for different stress levels (Fig. 15). The data were named according to the number of
351 cycles N and the corresponding Δq values. It appears that an increasing trend of M_r
352 with f_v can be identified for all stress levels. Moreover, this increasing trend followed
353 a bi-linear pattern with the slope at $f_v \geq 35\%$ larger than the one at $f_v \leq 20\%$,
354 evidencing that the soil fabrics of the ballast specimens at these two f_v ranges were
355 different: fine-fine contact structure at low f_v and grain-grain contact structure at

356 higher f_v . Same bi-linear variation trend of M_r was identified by Wang et al. [42] for
357 the microballast specimens, similarly, evidencing that the soil fabrics of microballast
358 specimens at $f_v \leq 20\%$ and $f_v \geq 35\%$ were separately dominated by fine-fine contact
359 structure and grain-grain contact structure.

360

361 **4.3. Comparison of permanent strain between ballast and microballast** 362 **specimens**

363 The estimated permanent strains for cycle $N = 90,000$ (end-stage cycle) at six f_v values
364 are presented in Fig. 16 for the ballast and the microballast specimens, for five stress
365 levels (10, 15, 20, 25 and 30 kPa). It can be observed that in the case of $f_v = 0\%$, at
366 each stress level, the ε_{1p} value of the ballast specimen coincides well with that of the
367 microballast specimen. For the fine-fine contact structure at $f_v = 5\%$ and 10% , on the
368 whole, the ε_{1p} values of the corresponding different scale specimens are found to be
369 similar. This phenomenon can be explained by the fact that in this case the fines
370 matrix constitutes the soil skeleton and the permanent strain was dominated by the
371 compression of the fines, giving rise to the permanent strains which were independent
372 of coarse grain size. For the grain-grain contact structure at $f_v = 35\%$ and 45% , it can
373 be observed that the permanent strains of the ballast specimens and the microballast
374 specimens were almost the same (Fig. 16), in particular at $\Delta q = 10$ kPa (Fig. 16a).
375 Note that although the case at $f_v = 20\%$ was categorized into the group of fine-fine
376 contact structure, the influence of coarse grain size on the permanent strain followed
377 the same pattern. This can be explained by the fact that at $f_v = 20\%$, part of the coarse

378 grains started to be in contact with each other. Further examination shows that at Δq
379 higher than 10 kPa, the strains of microballast specimens were slightly larger than
380 those of the ballast specimens. This phenomenon can be explained as follows: upon
381 loadings, the grains would slide into the pores nearby, giving rise to permanent strain.
382 If the difficulty of sliding into large pores for the large grains was the same as that for
383 the smaller grains to slide into smaller pores, identical permanent strains can be
384 expected. It is the case for the ballast specimen and the microballast specimen at $\Delta q =$
385 10 kPa. Apparently, the grains sliding depended on the stress level and the grain sizes;
386 in the microballast specimen, the grains with smaller sizes would slide into the
387 adjacent pores more easily, leading to a slightly larger strain.

388 Another possible explanation for the slightly larger strains in the microballast
389 specimen is related to the effect of the fines soils. As shown in Fig. 17, the fines soils
390 can be roughly considered to be distributed at two locations: the pores near the coarse
391 grain and the coarse grain intervals along the stress chain (supposed to be along the
392 specimen height). The applied load was transmitted along the stress chain by
393 compressing the fines between grains. When the load reached a certain level, grain
394 rearrangement occurred [26,27]. It can be inferred that the fines in the pores inhibited
395 the coarse grain sliding, while those between grains promoted it. At a given f_v value,
396 for the microballast specimen, more grain-fines-grain contacts can be expected along
397 the stress chain, leading to more distribution of fines soils. As a result, relatively
398 larger permanent strain can be expected.

399 As the difference of permanent strain between the two scale specimens appears

400 quite small (Figure. 16), it can be reasonably concluded that the parallel gradation
401 method is valid for the ballast/fines mixture in terms of permanent strain.

402

403 **4.4. Comparison of resilient modulus between ballast and microballast specimens**

404 The comparison of M_r values between the microballast and ballast specimens with
405 fine-fine contact structure is shown in Fig. 18. At $f_v = 0\%$, the M_r values of the ballast
406 specimen were comparable with those of the microballast specimen. This was normal
407 because the scaling question was not involved in that case. For higher f_v values, except
408 $f_v = 10\%$, the M_r values of the ballast and the microballast specimens coincided with
409 each other. The singular case at $f_v = 10\%$ was probably due to a technical problem.

410 The M_r values of the ballast specimens at grain-grain contact structure were
411 compared with those of the microballast specimens in Fig. 19 (Fig. 19a for $f_v = 35\%$
412 and Fig. 19b for $f_v = 45\%$). It can be observed that almost the same M_r values were
413 obtained for the two specimens, indicating that the resilient modulus was independent
414 of grain size. Further investigation shows that on the whole the M_r values of the
415 microballast specimens were slightly smaller than those of the ballast specimens.
416 These phenomena can be explained based on the analysis of Yang and Gu [48]. They
417 derived the resilient modulus of a simple cubic array of identical spheres under a
418 certain confining pressure by applying a small shear stress onto it. In the analysis, the
419 induced resilient shear strain of the cubic array was determined by adding up the
420 tangential strains between every two spheres along the vertical stress chain. This
421 tangential strain was calculated using the Hertz-Mindlin contact law, which was a

422 function of the applied shear stress. The expression for the resilient modulus (defined
423 as the ratio of the shear stress to the shear strain) was obtained, showing no
424 dependence on sphere radius. Note that this analysis did not consider any contribution
425 from fine soils, thus not fully reflecting the case of this study. Indeed, as mentioned
426 previously, in the case of mixture, the resilient modulus is affected by the fine soils
427 along the stress chain. For the microballast specimens, as stated before, there are more
428 fines soils along it. Thus, relatively smaller resilient modulus values are expected.

429 As for the permanent strain, globally, the resilient modulus also showed a good
430 agreement between the two scale specimens albeit the slight difference discussed
431 above, which validates the parallel gradation method in terms of resilient modulus.

432

433 **5. Conclusions**

434 The parallel gradation method was assessed on coarse grain/fines mixture by
435 comparing the mechanical parameters (permanent strain and resilient modulus) of the
436 two different scale specimens. Six volumetric coarse grain contents were considered
437 for each kind of specimens. Based on the results obtained, the following conclusions
438 can be drawn.

439 Two soil fabrics could be defined as fine-fine contact structure at $f_v = 0-20\%$
440 and grain-grain contact structure at $f_v = 35-45\%$. It was observed that for the ballast
441 and microballast specimens, with the increase of f_v value, the permanent strain
442 decreased rapidly when $f_v \leq 20\%$ and this decreasing rate slowed down when $f_v \geq 35\%$,
443 while the resilient modulus increased slightly when $f_v \leq 20\%$ and increased

444 significantly when $f_v \geq 35\%$.

445 The consistency between the large-scale and small-scale triaxial tests were
446 found to be satisfactory: at $f_v = 0\%$, the permanent strain as well as the resilient
447 modulus values obtained from the two scales showed a good correspondence. In the
448 case of fine-fine contact structure, the parallel gradation method was found to be valid.
449 The permanent strain and resilient modulus values of the ballast specimens were
450 consistent with the respective ones of the microballast specimens. This could be
451 explained by the fact that in this case the fines matrix governed the soil structure.

452 In the case of grain-grain contact structure, on the whole, the permanent strains
453 of the ballast specimens coincided with those of the microballast specimens
454 (especially at $\Delta q = 10$ kPa). This coincidence was also observed in terms of resilient
455 modulus. For the permanent strain, it could be explained by the fact that the
456 difficulties of the sliding of large ballast grains into the adjacent large pores and the
457 sliding of the small microballast grains into the smaller pores were expected to be the
458 same. For the resilient modulus, it could be explained by the analytical results of Yang
459 and Gu (2013), showing that the resilient modulus is independent of grain size.
460 Further examination showed that there were slight differences of permanent strain and
461 resilient modulus between two different scale specimens, which could be attributed to
462 the irregular grain sliding and the fines distribution.

463

464 **Acknowledgements**

465 The support from the Chinese Scholar Council (CSC) is greatly acknowledged.

467 **Notations**

A	constant in the similitude equation from ballast to microballast
D^b	given grain size of ballast
D_{\max}^b	maximum grain size of ballast
D_{\min}^b	minimum grain size of ballast
D^m	given grain size of microballast
D_{\max}^m	maximum grain size of microballast
D_{\min}^m	minimum grain size of microballast
f_v	volumetric content of coarse grains
M_r	resilient modulus
N	number of cycles
q	deviator stress
q_{\max}	maximum deviator stress
q_{\min}	minimum deviator stress
$w_{\text{opt-f}}$	optimum water content of fines
Δq	deviator stress amplitude
$\delta \varepsilon_{1p}^{M+1}$	translated permanent strain from the measured curve of Loading level M+1
ε_1	axial strain

ε_{1p}	permanent axial strain
ε_{1r}	resilient strain
ε_{1p}^M	measured permanent strain of the Loading Level M
ε_{1p}^{M+1}	estimated permanent strain of Loading level $M+1$
$\rho_{\text{dmax-f}}$	maximum dry density of fines

468

469 **References**

- 470 [1] Aingaran, S. 2014. Experimental investigation of static and cyclic behavior of
471 scaled railway ballast and the effect of stress reversal. Ph.D. thesis, University of
472 Southampton.
- 473 [2] Atkinson, J.H. 2000. Non-linear soil stiffness in routine design. *Géotechnique*,
474 50(5): 487-507.
- 475 [3] ASTM. 2011. D2487-11: Standard practice for classification of soils for
476 engineering purposes (unified soil classification system). ASTM International,
477 West Conshohocken, PA, USA.
- 478 [4] ASTM. 2012. D698-12: Standard test methods for laboratory compaction
479 characteristics of soil using standard effort. ASTM International, West
480 Conshohocken, PA, USA.
- 481 [5] Cai, Y.Q., Chen, J.Y., Cao, Z.G., Gu, C., and Wang, J. 2018. Influence of grain
482 gradation on permanent strain of unbound granular materials under low confining
483 pressure and high-cycle loading. *International Journal of Geomechanics*, 18(3):
484 04017156.

- 485 [6] Cao, Z.G., Chen, J.Y., Cai, Y.Q., Zhao, L., Gu, C., and Wang, J. 2018. Long-term
486 behavior of clay-fouled unbound granular materials subjected to cyclic loadings
487 with different frequencies. *Engineering Geology*, 243: 118-127.
- 488 [7] Cui, Y.J., Duong, T.V., Tang, A.M., Dupla, J.C., Calon, N., and Robinet, A. 2013.
489 Investigation of the hydro-mechanical behavior of fouled ballast. *Journal of*
490 *Zhejiang University-Science A (Applied Physics & Engineering)*, 14(4): 244-255.
- 491 [8] Duong, T.V. 2013. Investigation of the hydro-mechanical behavior of ancient
492 railway platforms in scope to reinforcement by soil-mixing. Ph.D. thesis, Ecole
493 Nationale des Ponts et Chaussées, Université Paris-Est.
- 494 [9] Duong, T.V., Cui, Y.J., Tang, A.M., Dupla, J.C., Canou, J., Calon, N., and Robinet,
495 A. 2016. Effects of water and fines contents on the resilient modulus of the
496 interlayer soil of railway substructure. *Acta Geotechnica*, 11(1): 51-59.
- 497 [10] Duong, T.V., Tang, A.M., Cui, Y.J., Trinh, V.N., Dupla, J.C., Calon, N., Canou, J.,
498 and Robinet, A. 2013. Effects of fines and water contents on the mechanical
499 behavior of interlayer soil in ancient railway sub-structure. *Soils and Foundations*,
500 53(6): 868-878.
- 501 [11] Dupla, J.C., Pedro, L.S., Canou, J., and Dormieux, L. 2007. Mechanical behavior
502 of coarse grained soils reference. *Bulletin de Liaison des Laboratoires des Ponts*
503 *et Chaussées*, 268-269: 31-58.
- 504 [12] Fagnoul, A., and Bonnechere, F. 1969. Shear strength of porphyry materials. *In*
505 *Proceedings of the 7th International Conference on Soil Mechanics and*
506 *Foundation Engineering, Mexico*, pp. 61-65.

- 507 [13] Gidel, G., Hornych, P., Chauvin, J.J., Breysse, D., and Denis, A. 2001. A new
508 approach for investigating the permanent deformation behavior of unbound
509 granular material using the repeated load triaxial apparatus. *Bulletin des*
510 *Laboratoires des Ponts et Chaussées*, 233: 5-21.
- 511 [14] Frost, R.J. 1973. Some testing experiences and characteristics of boulder-gravel
512 fills in earth dams. *In* Evaluation of relative density and its role in geotechnical
513 projects involving cohesionless soils. STP 523. ASTM Standards and
514 Publications.
- 515 [15] Grabe, P., and Clayton, C. 2009. Effects of principal stress rotation on permanent
516 deformation in rail track foundations. *Journal of Geotechnical and*
517 *Geoenvironmental Engineering*, 135(4): 555–565.
- 518 [16] Indraratna, B., Wijewardena, L.S.S., and Balasubramaniam, A.S. 1993.
519 Large-scale triaxial testing of greywacke rockfill. *Géotechnique*, 43: 37-51.
- 520 [17] Indraratna, B., Su, L., and Rujikiatkamjorn, C. 2011. A new parameter for
521 classification and evaluation of railway ballast fouling. *Canadian Geotechnical*
522 *Journal*, 48(2): 322-326.
- 523 [18] Jain, V., and Keshav, K. 1999. Stress distribution in railway formation - a
524 simulated study. *In* Proceeding of the 2nd International Symposium on Pre-Failure
525 Deformation Characteristics of Geomaterials-IS Torino.
- 526 [19] Jing, P., Nowamooz, H., and Chazallon, C. 2016. Permanent deformation
527 behaviour of a granular material used in low-traffic pavements. *Road Materials*
528 *and Pavement Design*, 19(2): 289-314.

- 529 [20] Lamas-Lopez, F., Costa D'Aguiar, S., Robinet, A., Cui, Y.J., Calon, N., Canou, J.,
530 Dupla, J.C., and Tang, A.M. 2015. In-situ investigation of the behaviour of a
531 French conventional railway platform. *In* Proceedings of Transportation Research
532 Board TRB 2015, Washington, DC.
- 533 [21] Lamas-Lopez, F. 2016. Field and laboratory investigation on the dynamic
534 behaviour of conventional railway track-bed materials in the context of traffic
535 upgrade. Ph.D. thesis, Ecole Nationale des Ponts et Chaussées, Université
536 Paris-Est.
- 537 [22] Lenart, S., Koseki, J., Miyashita, Y., and Sato, T. 2014. Large-scale triaxial tests
538 of dense gravel material at low confining pressures. *Soils and Foundation*, 54(1):
539 45-55.
- 540 [23] Li, D., and Selig, E. 1998. Method for railroad track foundation design. I:
541 Development. *Journal of Geotechnical and Geoenvironmental Engineering*,
542 124(4): 316–322.
- 543 [24] Lowe, J. 1964. Shear strength of coarse embankment dam materials. *In*
544 *Proceedings of the 8th International Congress on Large Dams 3*, Edinburgh, U.K.,
545 pp. 745-761.
- 546 [25] Nitchiporovitch, A.A. 1969. Shearing strength of coarse shell materials. *In*
547 *Proceedings of the 7th International Conference on Soil Mechanics and*
548 *Foundation Engineering*, Mexico, pp. 211-216.
- 549 [26] Oda, M., Konishi, J., and Nasser, N.S. 1982. Experimental micromechanical
550 evaluation of strength of granular materials: effects of particle rolling. *Mechanics*

- 551 of Materials, 1(4): 269-283.
- 552 [27] Oda, M., and Kazama, H. 1998. Microstructure of shear band and its relation to
553 the mechanisms of dilatancy and failure of dense granular soils. *Géotechnique*,
554 48(4): 465-481.
- 555 [28] Pedro, L. 2004. De l'étude du comportement mécanique de sols hétérogènes
556 modèles à son application au cas des sols naturels. Ph.D. thesis, Ecole Nationale
557 des Ponts et Chaussées, Université Paris-Est.
- 558 [29] Qi, S., Cui, Y.J., Chen, R.P., Wang, H.L., Lamas-Lopez, F., Aïmediou, P., Dupla,
559 J.C., Canou, J., and Saussine, G. 2019. Influence of grain size distribution of
560 inclusions on the mechanical behaviors of track-bed materials. *Géotechnique in*
561 *press*. doi : 10.1680/jgeot.18.P.047.
- 562 [30] Rollins, K.M., Evans, M.D., Diehl, N.B., and Daily III, W.D. 1998. Shear
563 modulus and damping relationships for gravels. *Journal of Geotechnical and*
564 *Geoenvironmental Engineering*, 124(5): 396-405.
- 565 [31] Seed, H.B., Wong, R.T., Idriss, I.M., and Tokimatsu, K. 1986. Moduli and
566 damping factors for dynamic analyses of cohesionless soils. *Journal of*
567 *Geotechnical Engineering*, 112(11): 1016-1032.
- 568 [32] Seif El Dine, B., Dupla, J.C., Frank, R., Canou, J., and Kazan, Y. 2010.
569 Mechanical characterization of matrix coarse-grained soils with a large-sized
570 triaxial device. *Canadian Geotechnical Journal*, 47: 425-438.
- 571 [33] Selig, E., and Waters, J. 1994. Track geotechnology and sub-structure
572 management. Thomas Telford, London, U.K.

- 573 [34] Sevi, A., and Ge, L. 2012. Cyclic behaviors of railroad ballast within the parallel
574 gradation scaling framework. *Journal of Materials in Civil Engineering*, 24(7):
575 797-804.
- 576 [35] Suiker, A.S.J., Selig, E.T., and Frenkel, R. 2005. Static and cyclic triaxial testing
577 of ballast and subballast. *Journal of Geotechnical and Geoenvironmental*
578 *Engineering*, 131: 771-782.
- 579 [36] Tang, L., Yan, M.H., Ling, X.Z., and Tian, S. 2017. Dynamic behaviours of
580 railway's base course materials subjected to long-term low-level cyclic loading:
581 experimental study and empirical model. *Géotechnique*, 67(6): 537-545.
- 582 [37] Trinh, V.N. 2011. Comportement hydromécanique des matériaux constitutifs de
583 plateformes ferroviaires anciennes. Ph.D. thesis, Ecole Nationale des Ponts et
584 Chaussées, Université Paris-Est.
- 585 [38] Trinh, V.N., Tang, A.M., Cui, Y.J., Dupla, J.C., Canou, J., Calon, N., Lambert, L.,
586 Robinet, A., and Schoen, O. 2012. Mechanical characterisation of the fouled
587 ballast in ancient railway track sub-structure by large-scale triaxial tests. *Soils*
588 *and Foundations*, 52(3): 511-523.
- 589 [39] Varadarajan, A., Sharma, K.G., Venkatachalam, K., and Gupta, A.K. 2003.
590 Testing and modeling two rockfill materials. *Journal of Geotechnical and*
591 *Geoenvironmental Engineering*, 129(3): 206-218.
- 592 [40] Wang, H.L., and Chen, R.P. 2019. Estimating static and dynamic stresses in
593 geosynthetic-reinforced pile-supported track-bed under train moving loads.
594 *Journal of Geotechnical and Geoenvironmental Engineering*, 145(7): 04019029.

- 595 [41] Wang, H.L., Chen, R.P., Cheng, W., Qi, S., and Cui, Y.J. 2019. Full-scale model
596 study on variations of soil stress in geosynthetic-reinforced pile-supported
597 track-bed with water level change and cyclic loading. *Canadian Geotechnical*
598 *Journal*, 56(1): 60–68.
- 599 [42] Wang, H.L., Cui, Y.J., Lamas-Lopez, F., Dupla, J.C., Canou, J., Calon, N.,
600 Saussine, G., Aïmediou, P., and Chen, R.P. 2017. Effects of inclusion contents on
601 resilient modulus and damping ratio of unsaturated track-bed materials. *Canadian*
602 *Geotechnical Journal*, 54: 1672-1681.
- 603 [43] Wang, H.L., Cui, Y.J., Lamas-Lopez, F., Dupla, J.C., Canou, J., Calon, N.,
604 Saussine, G., Aïmediou, P., and Chen, R.P. 2018a. Permanent deformation of
605 track-bed materials at various inclusion contents under large number of loading
606 cycles. *Journal of Geotechnical and Geoenvironmental Engineering*, 144(8):
607 04018044.
- 608 [44] Wang, H.L., Cui, Y.J., Lamas-Lopez, F., Calon, N., Saussine, G., Dupla, J.C.,
609 Canou, J., Aïmediou, P., and Chen, R.P. 2018b. Investigation on the mechanical
610 behavior of track-bed materials at various contents of coarse grains. *Construction*
611 *and Building Materials journal*, 164: 228-237.
- 612 [45] Werkmeister, S., Dawson, A.R., and Wellner, F. 2004. Pavement design model for
613 unbound granular materials. *Journal of Transportation Engineering*, 130:
614 665-674.
- 615 [46] Wichtmann, T., Rondon, H.A., Niemunis, A., Triantafyllidis, Th., and Lizcano, A.
616 2010. Prediction of permanent deformations in pavements using a high-cycle

617 accumulation model. *Journal of Geotechnical and Geoenvironmental Engineering*,
618 136: 728-740.

619 [47] Xiao, Y., Liu, H.L., Chen, Y.M., and Jiang, J.S. 2014. Bounding surface model
620 for rockfill materials dependent on density and pressure under triaxial stress
621 conditions. *Journal of Engineering Mechanics*, 140: 04014002.

622 [48] Yang, J., and Gu, X.Q. 2013. Shear stiffness of granular material at small strains:
623 does it depend on grain size?. *Géotechnique*, 63(2): 165-179.

624 [49] Yang, L., Powrie, W., and Priest, J. 2009. Dynamic stress analysis of a ballasted
625 railway track bed during train passage. *Journal of Geotechnical and*
626 *Geoenvironmental Engineering*, 135(5): 680–689.

627 [50] Zeller, J., and Wullimann, R. 1957. The shear strength of the shell materials for
628 the Göschenalp Dam, Switzerland. *In Proceedings of the 4th International*
629 *Conference on Soil Mechanics and Foundation Engineering*, London, pp.
630 399-404.

List of tables

Table 1. Mass proportions and grain size ranges of nine commercial soils

List of Figures

Fig. 1. Grain size distributions of the ballast and the microballast (modified from Wang et al. 2018a)

Fig. 2. Grain size distributions of fines (modified from Wang et al. 2018a)

Fig. 3. Typical sine-shaped signals applied in the cyclic loadings

Fig. 4. Loading paths in two stages: (a) stage 1 for permanent strain investigation; (b) stage 2 for resilient modulus investigation

Fig. 5. Deviator stress q versus axial strain ε_1 for the first 90,000 cycles of loading stage 1 (ballast specimen at $f_v = 35\%$)

Fig. 6. Permanent strain evolutions with number of cycles at different f_v values (ballast specimens)

Fig. 7. Illustration of the method to eliminate the loading history effect

Fig. 8. Measured and estimated permanent strain curves for ballast specimen at $f_v = 0\%$

Fig. 9. Estimated permanent strain evolutions at the first 90,000 cycles for ballast specimen at $f_v = 0\%$

Fig. 10. Variations of estimated end-stage permanent strains with f_v at different stress levels (ballast specimens)

Fig. 11. Hysteresis loops at first cycles of different stress levels for ballast specimen at

$f_v = 20\%$: $\Delta q = 10$ kPa (N = 1), $\Delta q = 30$ kPa (N = 101), $\Delta q = 50$ kPa (N = 201), $\Delta q = 100$ kPa (N = 701) and $\Delta q = 200$ kPa (N = 1401)

Fig. 12. Hysteresis loops during 100 cycles (N = 701 to 800) under $\Delta q = 100$ kPa for ballast specimen at $f_v = 20\%$

Fig. 13. Determination of M_r

Fig. 14. Evolution of M_r with number of cycles at different stress levels for ballast specimen at $f_v = 20\%$

Fig. 15. Evolutions of M_r at end stage with f_v for ballast specimens at: (a) $\Delta q = 10$ kPa; (b) $\Delta q = 30$ kPa; (c) $\Delta q = 50$ kPa; (d) $\Delta q = 100$ kPa and 200 kPa

Fig. 16. Variations of estimated end-stage permanent strains with f_v for ballast and microballast specimens at: (a) $\Delta q = 10$ kPa; (b) $\Delta q = 15$ kPa; (c) $\Delta q = 20$ kPa; (d) $\Delta q = 25$ kPa and 30 kPa

Fig. 17. Schematic illustration of the distribution of fines soils in case of grain-grain contact structure

Fig. 18. Comparison of M_r value between ballast specimens and microballast specimens in case of fine-fine contact structure for: (a) $f_v = 0\%$; (b) $f_v = 5\%$; (c) $f_v = 10\%$; (d) $f_v = 20\%$

Fig. 19. Comparison of M_r value between ballast specimens and microballast specimens in case of grain-grain contact structure for (a) $f_v = 35\%$ and (b) $f_v = 45\%$

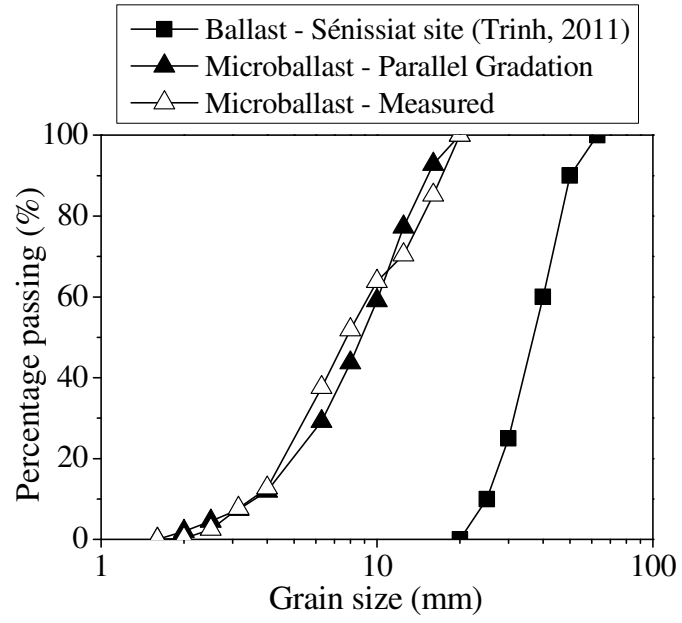


Fig. 1. Grain size distributions of the ballast and the microballast (modified from Wang et al. 2018a)

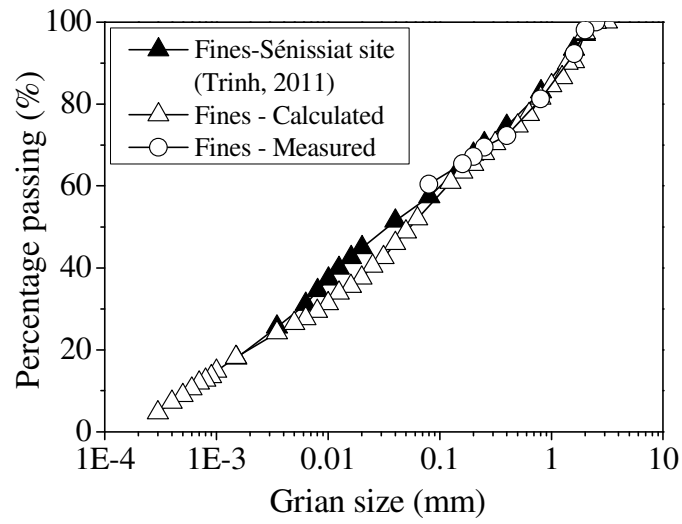


Fig. 2. Grain size distributions of fines (modified from Wang et al. 2018a)

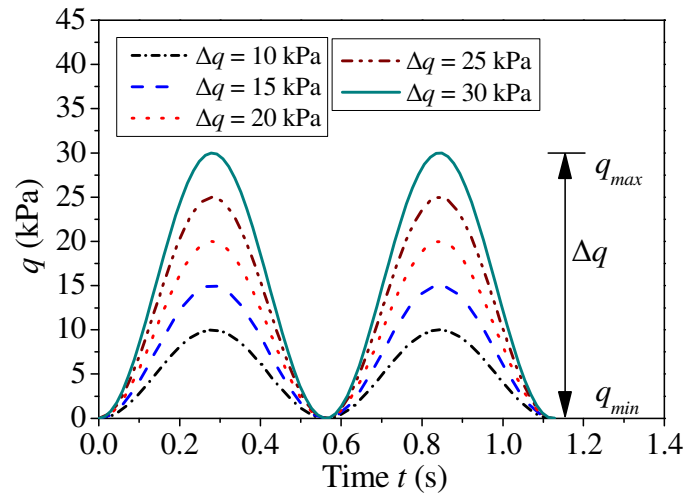


Fig. 3. Typical sine-shaped signals applied in the cyclic loadings

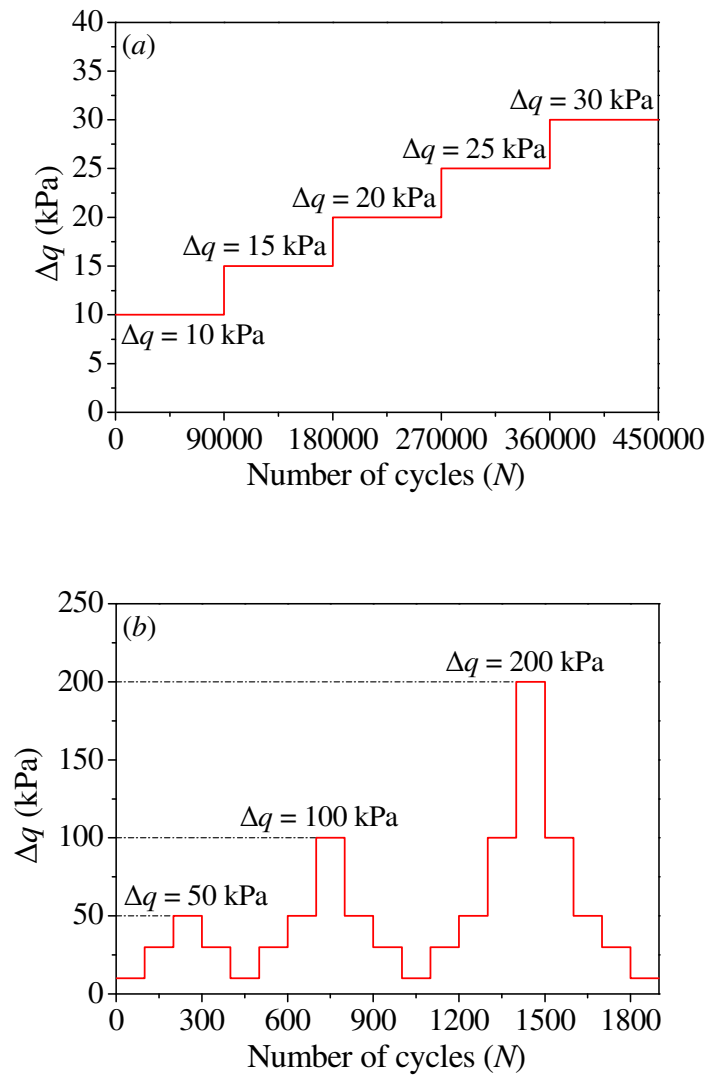


Fig. 4. Loading paths in two stages: (a) stage 1 for permanent strain investigation; (b) stage 2 for resilient modulus investigation

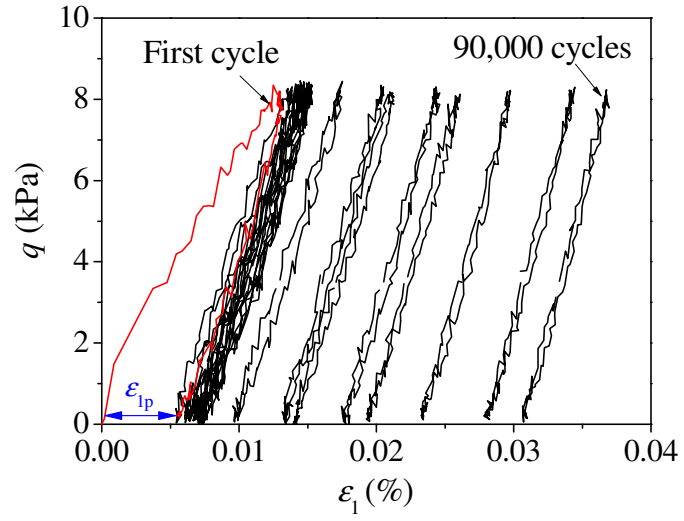


Fig. 5. Deviator stress q versus axial strain ε_1 for the first 90,000 cycles of loading stage 1 (ballast specimen at $f_v = 35\%$)

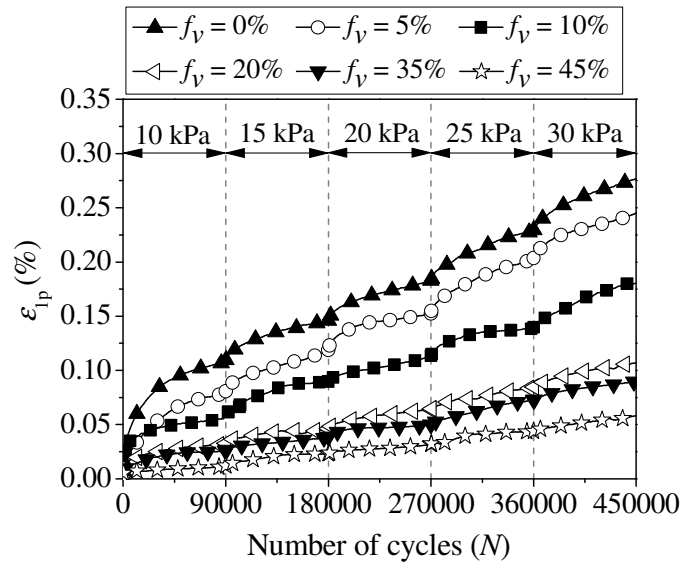


Fig. 6. Permanent strain evolutions with number of cycles at different f_v values

(ballast specimens)

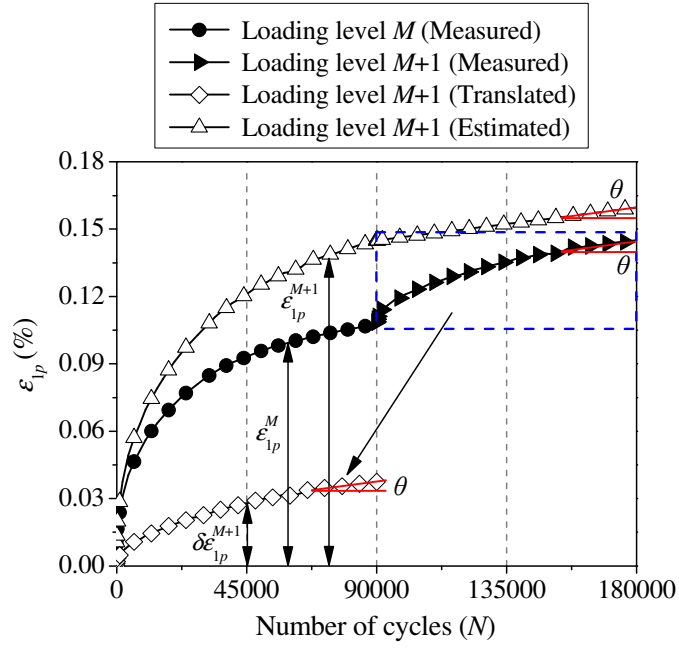


Fig. 7. Illustration of the method to eliminate the loading history effect

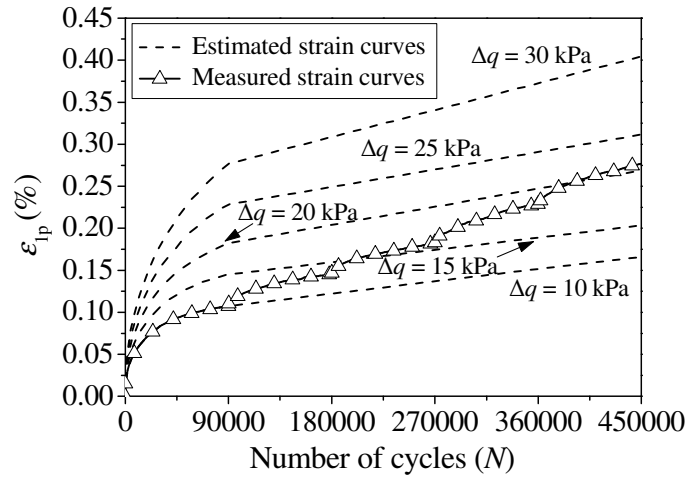


Fig. 8. Measured and estimated permanent strain curves for ballast specimen at $f_v =$

0%

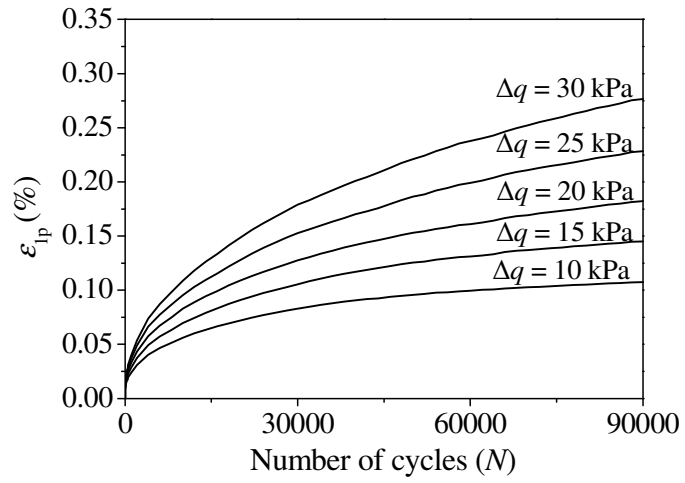


Fig. 9. Estimated permanent strain evolutions at the first 90,000 cycles for ballast specimen at $f_v = 0\%$

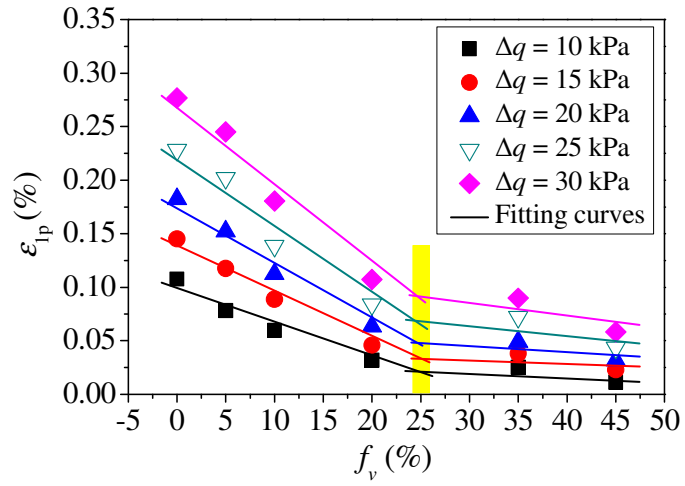


Fig. 10. Variations of estimated end-stage permanent strains with f_v at different stress levels (ballast specimens)

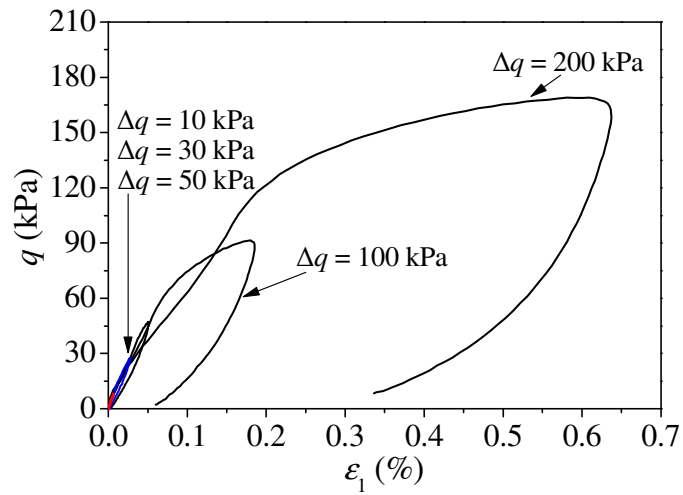


Fig. 11. Hysteresis loops at the first cycles of different stress levels for ballast specimen at $f_v = 20\%$: $\Delta q = 10$ kPa ($N = 1$), $\Delta q = 30$ kPa ($N = 101$), $\Delta q = 50$ kPa ($N = 201$), $\Delta q = 100$ kPa ($N = 701$) and $\Delta q = 200$ kPa ($N = 1401$)

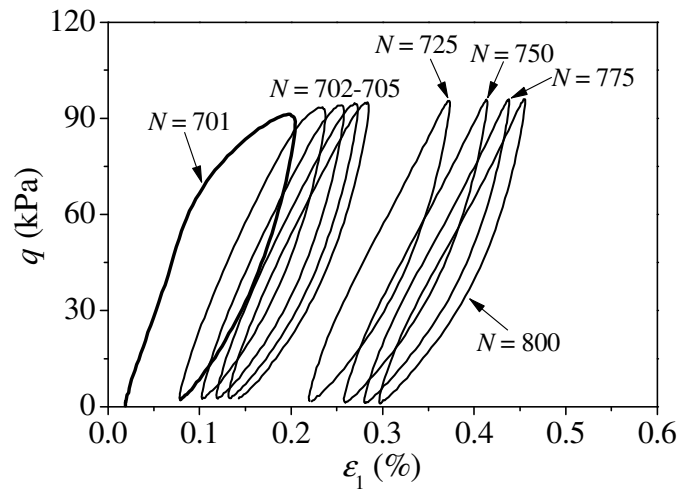


Fig. 12. Hysteresis loops during 100 cycles ($N = 701$ to 800) under $\Delta q = 100$ kPa for ballast specimen at $f_v = 20\%$

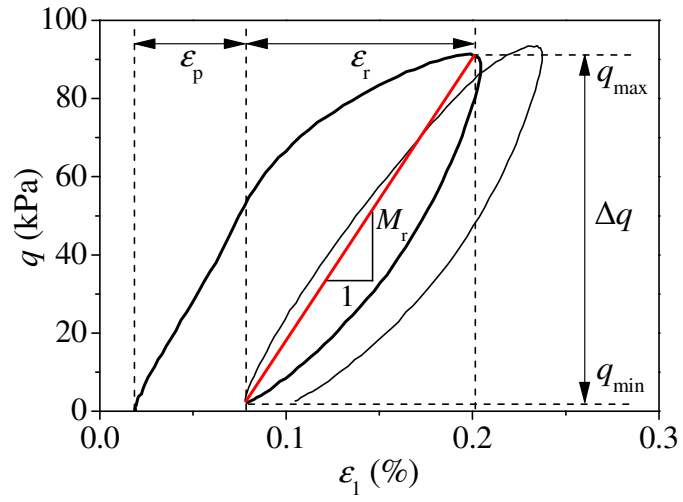


Fig. 13. Determination of M_r

Note: The two hysteresis loops shown are the testing results of ballast specimen at $f_v = 20\%$ under $\Delta q = 100$ kPa at cycle numbers of $N = 701$ and 702 .

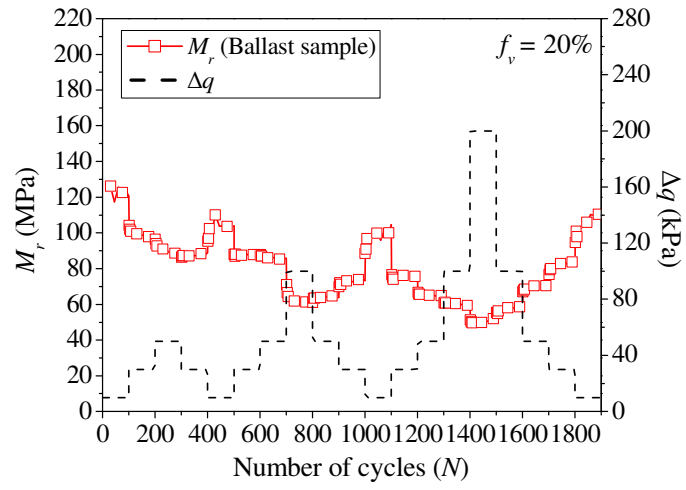


Fig. 14. Evolution of M_r with number of cycles at different stress levels for ballast specimen at $f_v = 20\%$

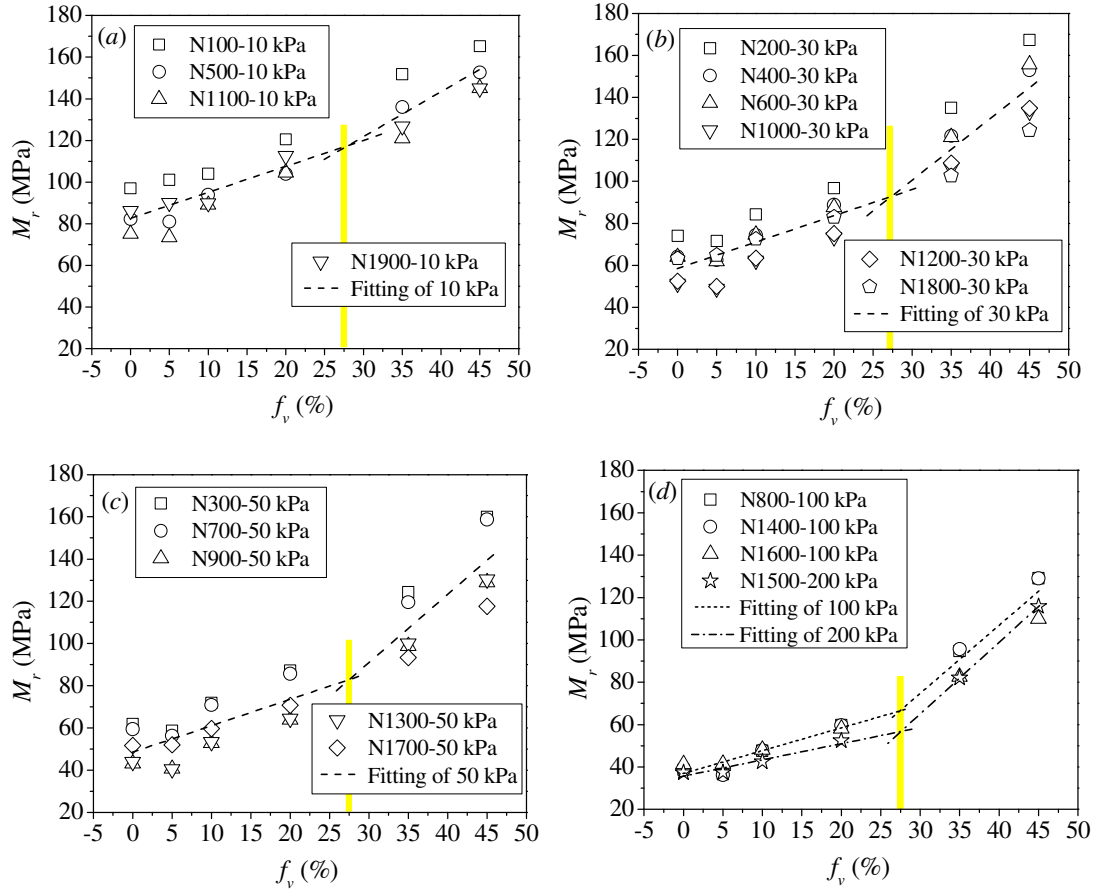


Fig. 15. Evolutions of M_r at end stage with f_v for ballast specimens at: (a) $\Delta q = 10$ kPa;

(b) $\Delta q = 30$ kPa; (c) $\Delta q = 50$ kPa; (d) $\Delta q = 100$ kPa and 200 kPa

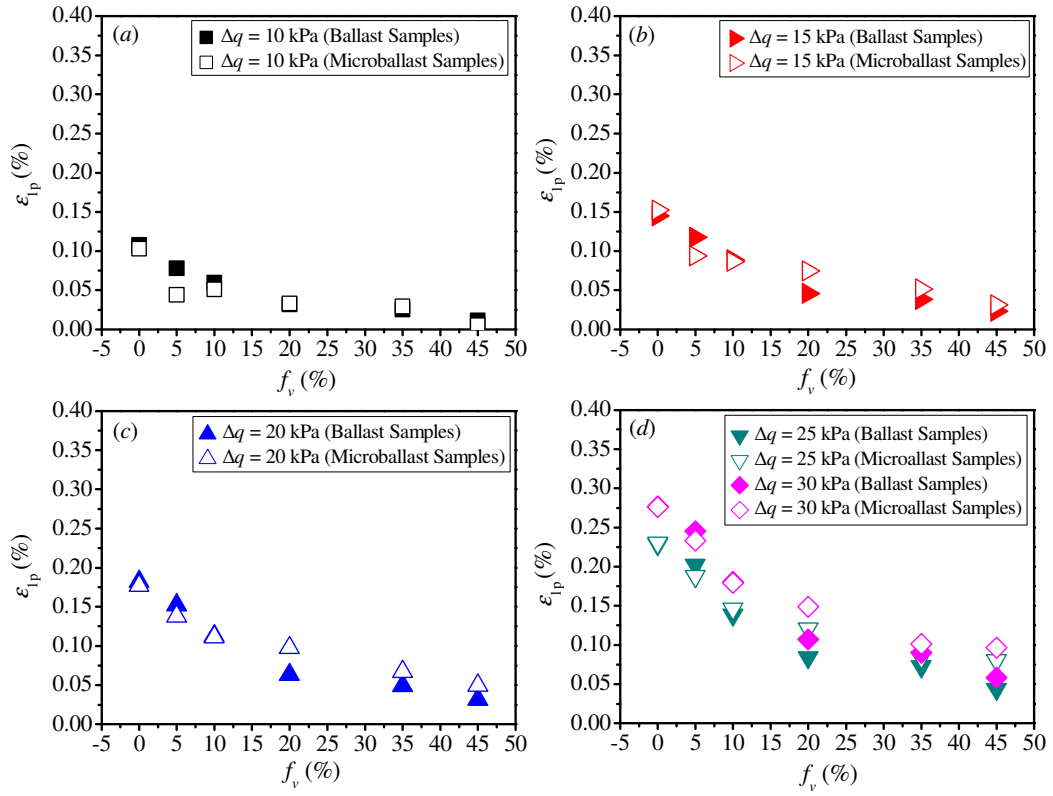


Fig. 16. Variations of estimated end-stage permanent strains with f_v for ballast and microballast specimens at: (a) $\Delta q = 10$ kPa; (b) $\Delta q = 15$ kPa; (c) $\Delta q = 20$ kPa; (d) $\Delta q = 25$ kPa and 30 kPa

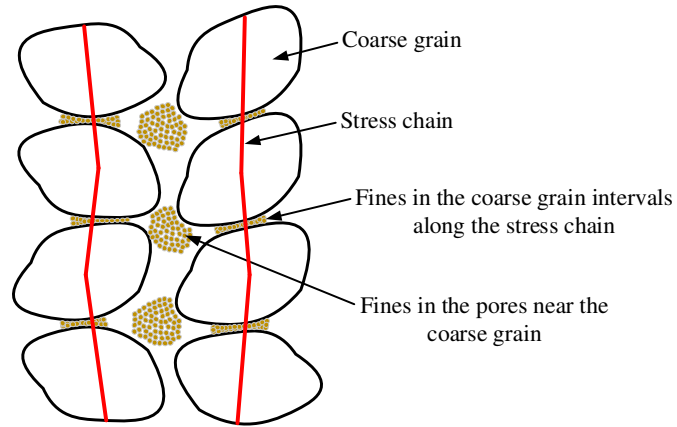


Fig. 17. Schematic illustration of the distribution of fines soils in case of grain-grain contact structure

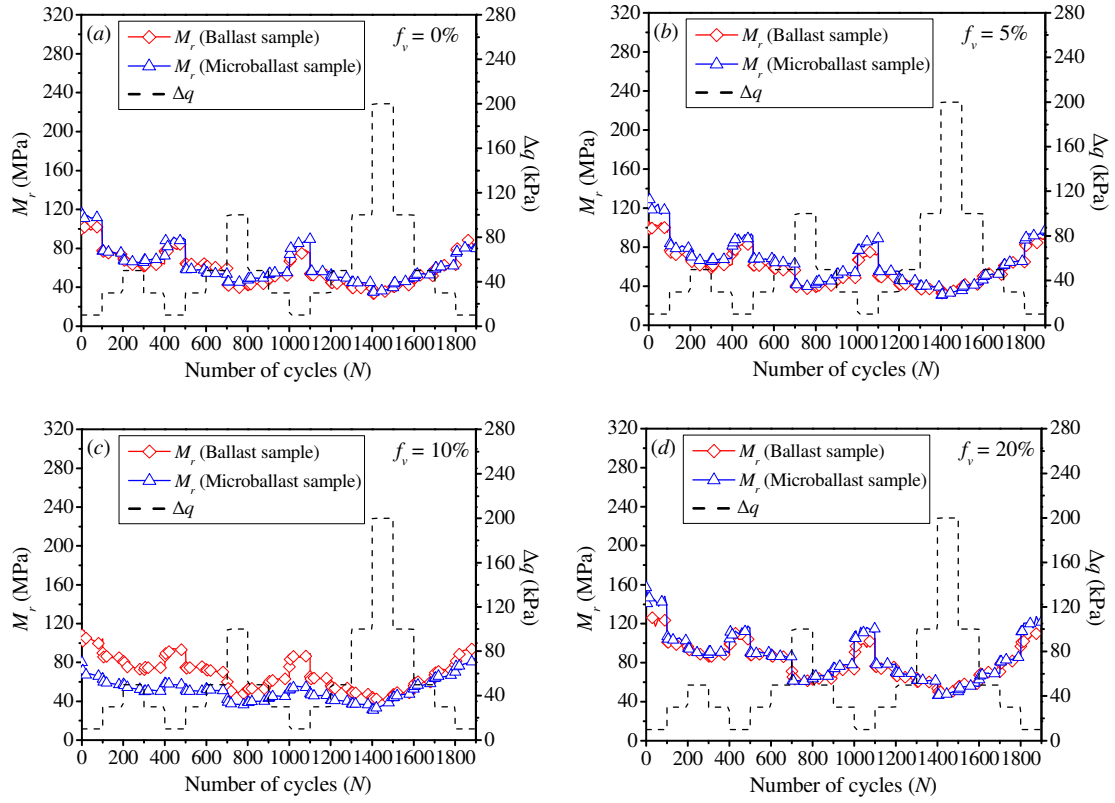


Fig. 18. Comparison of M_r value between ballast specimens and microballast specimens in case of fine-fine contact structure for: (a) $f_v = 0\%$; (b) $f_v = 5\%$; (c) $f_v = 10\%$; (d) $f_v = 20\%$

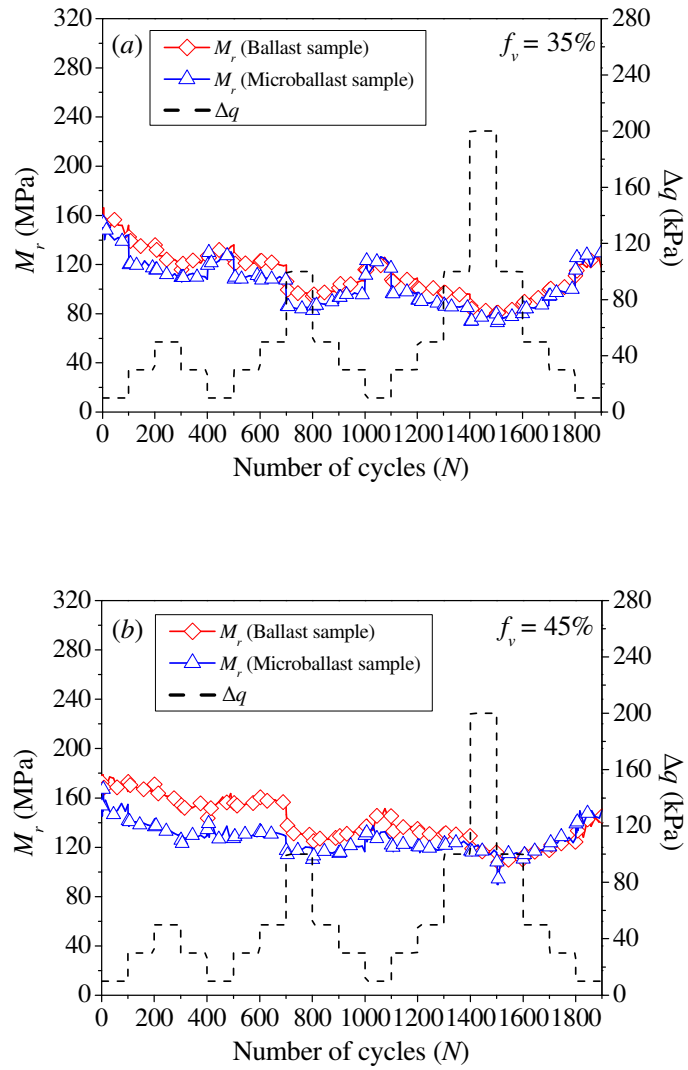


Fig. 19. Comparison of M_r value between ballast specimens and microballast specimens in case of grain-grain contact structure for (a) $f_v = 35\%$ and (b) $f_v = 45\%$

Table 1. Mass proportions and grain size ranges of nine commercial soils

0.001 - 0.01 (20% of the particles)

0.0003 - 0.01 (80% of the particles)

0.0009 - 0.25

0.0009 - 0.50

0.063 - 0.50

0.16 - 0.63

0.25 - 1

0.32 - 2

0.32 - 3.20
